







Predicting the Level of Co-Activation of One Muscle Head from the Other Muscle Head of the *Biceps Brachii* Muscle by Linear Regression and Shallow Feedforward Neural Networks

Nils Grimmelmann^{1,2,*}^a, Malte Mechtenberg^{1,2}^b, Markus Vieth³^c, Alexander Schulz³^d,
Barbara Hammer³^e and Axel Schneider^{1,2}^f

¹*Biomechanics and Embedded Systems Group, University of Applied Sciences and Arts, Bielefeld, Germany*

²*Institute of System Dynamics and Mechatronics, University of Applied Sciences and Arts, Bielefeld, Germany*

³*Machine Learning Group, Bielefeld University, Bielefeld, Germany*


Keywords: sEMG, Muscle Model, Limb Movement Prediction, Virtual Sensor, Linear Regression, Regression.


Abstract: One of the challenges in close-to-body robotics is the intuitive control of exoskeletal devices which requires lag-free responses of its actuated joints. A frequently used signal domain to satisfy the required control properties is surface electromyography (sEMG). By using a Hill-type model of the muscle mainly responsible for the movement of a biological joint, which is excited by the corresponding sEMG of this muscle, the joint movement can be pre-calculated. If the muscle internal delays are used, this information can be used for an intuitive and lag-free control. So far, biomechanical limb and joint models including Hill-type muscle sub-model were used. In current studies, state-of-the-art machine learning models are evaluated for this problem. Both types, classical and machine learning models, depend on the measured sEMG signals of all muscle heads of a relevant muscle and on their respective signal quality. This work introduces a method to train a virtual sEMG-sensor as a replacement for the real sEMG signal of a muscle head, thus reducing the number of real sensor electrodes on a given muscle. The virtual sensor is trained based on data from the remaining sensor. This method allows to compare the measured sEMG signal with the virtual sensor output to assess the measured signal. Furthermore, this study explains the training process and evaluates the use of the virtual sensor in a biomechanical limb model.


1 INTRODUCTION


The use of active exoskeletons and wearables provides a way to support the wearer during force-intensive movements. This requires time critical motion prediction so that the active exoskeleton can be controlled in a way to follow the postures of the wearer without delay. Electromyography (EMG) signals provide a source of information for the required movement prediction which can also be measured before the muscle contracts and an actual limb movement or force interaction with the


exoskeleton occurs. EMG signals can be measured invasively with needles inserted into the muscle (Merletti and Farina, 2008). This method requires special medical knowledge on the correct insertion of the needle into the muscle. It provides measurements that are less affected by crosstalk, so the signal amplitude from the selected muscle head is higher than that from the surrounding muscle heads. The surface electromyography (sEMG), on the other hand, requires no special medical knowledge and is non-invasive. Measuring EMG on the surface of the skin means that only superficial muscles or muscle heads can be measured. Muscles or muscle heads that lie deep below other muscle tissue are less accessible with this measurement method. Therefore, not all muscles or muscle heads involved in a limb movement can be used in a model to predict the limb movement when sEMG is the source of information.


^a <https://orcid.org/0000-0002-4864-4978>

^b <https://orcid.org/0000-0002-8958-0931>

^c <https://orcid.org/0000-0003-1707-6231>

^d <https://orcid.org/0000-0002-0739-612X>

^e <https://orcid.org/0000-0002-0935-5591>

^f <https://orcid.org/0000-0002-6632-3473>

For example, if the movement of the forearm is considered via the elbow joint, which has one rotatory degree of freedom, mainly three muscles are used for flexing: the two-headed *biceps brachii*, the single-headed *brachioradialis* and the single-headed *brachialis*. The extension of the elbow is mainly performed by two muscles: the three-headed *triceps brachii* and the single-headed *anconeus*.

The two *biceps* heads (*biceps* short head and *biceps* long head) are located below the skin surface. Both muscle heads end distally in a common tendon. Proximally, each muscle head ends in its own tendon. The tendons terminate at different points on the shoulder bone, called *scapular*. Both heads can flex the elbow but also have secondary functions. The proximal tendon of the *biceps* long head wraps around the shoulder joint and stabilises the shoulder (Schünke et al., 2010).

As shown in previous work, limb movement can be predicted with only the two surface muscles *biceps* and *triceps*. Firstly, with a biomechanical limb model based on a Hill-type (Hill, 1964; Zajac, 1989) muscle model (Grimmelsmann et al., 2023). Secondly, with a purely data-driven (black box) approach (Leserri et al., 2022). Depending on the experiment and data set, a different set of the five main muscles involved in the flexion and extension of the elbow are used for elbow movement prediction (e.g. (Koo and Mak, 2005) uses *biceps*, *brachioradialis* and the *triceps*).

However, this work also shows that the signal quality and signal integrity can be different for two muscle heads of the same muscle, e.g. due to changing quality of the respective electrode skin contact. This can potentially lead to a failed prediction depending on the overall model structure. Due to the common distal tendon, both *biceps* heads show similarities in the time courses of their respective neuronal activation.

For this reason, a method is proposed that exploits the close similarity between the two *biceps* heads to create a virtual sensor for one head based only on the measurement of the sEMG of the other. This allows the use of only one sensor, namely the one with the better signal quality. In principle, the concept of a virtual sensor is also suited to derive unavailable sEMG measurements, e.g. of deep lying muscle heads, from easy to measure more superficially located muscle heads, if their common function suggests a similar activation in terms of time. To test the concept of a virtual sensor, this work follows the former of the above two applications and replaces one of the two *biceps* heads, although sEMG measurements of both superficially located heads are available. Here, the unknown signal quality of the

two measured heads is an additional challenge (see above). The signal of the virtual sensor for one head is derived by linear regression and shallow feedforward neural network (FFN) using the measurement of the other head. To reflect the secondary functions of the two heads, additional features are added as input to the regression. These additional features are related to the dynamics of the elbow and are the elbow angle, the upper arm angle (w.r.t. the gravitational vector) and the overall weight of lower arm plus hand and an additional weight (dumb bell). After the regression step, these virtual sensors are also used as input to the biomechanical limb model (domain-knowledge based model) to prove the suitability for the limb movement prediction. In previous works, different strategies were used to train virtual sensors. One approach is to use recurrent neural network (RNN) such as long short-term memory (LSTM) to estimate the virtual sEMG channel (Machado et al., 2019). This approach focuses mainly on the performance w.r.t. the classification of a hand movement and not on the interpretation of the underlying sEMG data. The method proposed in this work uses linear regression and shallow FFN.

Based on an extensive data set (Mechtenberg et al., 2023), the outputs of the virtual sensor can be compared with the neuronal activation calculated from the real sEMG measurements of the replaced muscle head on the one hand and evaluated w.r.t their contribution to the predicted joint movement on the other hand, as the virtual sensor output is fed into the model instead of the replaced head. To maintain interpretability the architecture/ complexity is gradually extended in this work. Besides interpreting the results of the virtual sensor, the sensor is also validated using a domain-knowledge based model.

Other methods such as (Kim et al., 2019) use virtual sensors for a signal-assisted classification. The general idea of using a trained regression for enhancing the signal integrity matches parts of our approach (sEMG assessment).

The methods section starts with an overview of the sEMG data set and the biomechanical model of the upper arm and the elbow joint. The internal signal neuronal activation from this model serves as a foundation for the domain knowledge-based feature used in the regression (section 2.2). A description of the different regression setups follows in section 2.3 and section 2.4. The virtual sensor will be used in a domain knowledge-based model. The explanation of the validation process for this purpose can be found in section 2.5. The methods section ends with an exemplary use case of the virtual sensor, the sEMG

post measurement assessment. The results of the two setups are discussed in section 3.1 and section 3.2. The results section also shows the validation results and the assessment for two different subjects.

2 METHODS

As a basis for understanding the nature of the data on which this study is based on (Mechtenberg et al., 2023), a brief summary of the experiments used to collect the data is given first. In these experiments, the sEMG of both *biceps* and the two *triceps* heads were recorded. The sEMG signals contain frequency components from about 10 Hz to 400 Hz (Merletti et al., 2018).

The periodic movement of the elbow (dumbbell curls), however, is at about 0.5 Hz. Because of this large difference in dynamics, the sEMG was not directly used as the target value of the virtual sensor regression. It is further converted into the activation of the muscle. In the domain model, this is achieved by a nonlinear low-pass filter that represents the activation dynamics of the muscle head (Zajac, 1989). The resulting signal thus has lower frequency components than the sEMG. The calculation of this activation dynamics is briefly described in section 2.2. In sections 2.3 and 2.4 a description of the two setups for learning the virtual sensor is presented. For validation of the virtual sensor, the sensor is used as a replacement input in a domain-knowledge based model (described in section 2.5). At the end of the methods section a potential use case (the sEMG post-measurement assessment) of the trained virtual sensor is described (see section 2.6).

2.1 sEMG Data Set and Biomechanical Overview

The used data set (Mechtenberg et al., 2023) involved 31 healthy subjects performing different motion sequences, with 29 choosing their right arm as their dominant arm and 2 choosing the left arm. They were randomly labeled with an identification number (subject id) starting from id=20. The subject ids [23, 27, 35] were not assigned. The positions of the *acromion* at the shoulder and the lateral *epicondyle* at the elbow were used as reference points to calculate the length of the upper arm. The positions of the medial *epicondyle* and the *processus styloideus ulnae* at the wrist were used to calculate the length of the forearm.

Two wireless sEMG sensors (Delsys Trigno, Delsys, Inc., Boston, MA, USA) were attached to

the skin surface above the *biceps brachii* and *triceps brachii*. The sensors used a sampling period of 900 μ s and 16-bit resolution. The sensors were applied such that their electrodes were placed on the muscle belly proximal to the innervation zone. The individual muscle heads of *biceps* and *triceps* were palpated by an experienced experimenter. A schematic representation of the two *biceps* heads is shown in fig. 1 (D). After the skin preparation and alignment, the sensors were attached to the subjects' skin with double-sided adhesive tape. The electrical quality of the interface between the skin and the electrodes was evaluated in a preliminary experiment by instructing the subjects to contract the flexors and extensors of the upper arm while the experimenter visually checked the signal quality.

A passive measurement orthosis was used to measure the elbow angle θ synchronously with sEMG recordings. The orthosis was custom-designed and 3D-printed in-house from PLA plastic so that it could be adapted to different arm sizes. The elbow angle was determined using a 10-bit magnetic rotary position encoder (AS5043, ams AG, Premstaetten, Austria) integrated into the joint and aligned to the subject's rotary axis of the elbow joint. The analog output was fed into a Trigno Analog Adapter for synchronous recording. Calibration was performed by the supervisor during the initial experiment. Figure 1(A) shows the measurement orthosis as well as the sEMG sensors.

All subjects performed the same movement sequences, which involved periodic movements of the dominant forearm. Two different postures of the upper arm were adopted and two different weighted dumbbells were used, which were held by the subject. The subjects were instructed to align the longitudinal axis of the forearm orthogonally to the longitudinal axis of the upper arm, resulting in an initial elbow angle of $\theta_0 = 90^\circ$. In the lower posture (see fig. 1 (B)), the upper arm was held vertically pointing downwards. In the upper posture, the upper arm was held vertically pointing upwards. For this study, only the lower posture (flexor muscles dominant) is used.

In the experiments, four different weights were held by the subject ($w = [2\text{ kg}, 4\text{ kg}]$). After the initial static phase with an elbow angle of $\theta_0 = 90^\circ$, subjects were instructed to move the forearm up and down rhythmically about the axis of the elbow joint at a constant angular velocity, resulting in a sine-like modulation of the elbow joint angle. After $\Delta t = 30\text{ s}$ of dynamic movement, subjects were instructed to stop and rest for at least one minute before repeating the trials with a different weight. For each weight, experiments were performed at [0.25 Hz (slow) and

0.5 Hz (fast)]. One experiment contained an unusual arm movement and was rejected (2kg, slow speed, id=50).

2.2 Domain Knowledge-Based Model for Feature Extraction and Virtual Sensor Validation

In perspective, the virtual sensor is intended to serve as an input for a biomechanical model for limb motion prediction. In the following method section different virtual sensors are trained. All virtual sensors predict a neuronal activation of one *biceps* head but have different training setups and input configurations. The biomechanical model used in section 3.3 for the validation is described in the following overview. A detailed description of all subsystems of the model can be found in (Grimmelsmann et al., 2023). Parts of this model were also used for the calculation of the neuronal activation from the sEMG signals.

The signal flow in the model shown in fig. 2 is from left to right. The model contains different submodels which represent the biological parts of muscle, joint, and biomechanics. From the left, four sEMG channels are shown, which are divided into subsystems. The upper path (two shades of red) represents the two *biceps* heads. The lower path (two shades of blue) represents the *triceps* heads. The original model also uses all 4 sEMG channels for validation in this work. However, the virtual sensors are only trained for *biceps* activation. Both paths converge on the right side of the figure to a torque that moves the elbow joint. The angle of the elbow joint is then calculated from the superimposed torque of the two muscles using the respective dynamics equations. This is usually used as a prediction signal.

Within the model, the neural activation is available at the output of the activation dynamics. Up to this point, the EMG signal has been processed in several steps. First, it was amplified by a factor of k . The amplified signal was then filtered with a 4th order Butterworth bandpass (cut-off frequencies of $f_{low} = 4\text{Hz}$ and $f_{high} = 400\text{Hz}$) (del Toro et al., 2019) to reduce noise. Rectification of the signal as introduced in (Zajac, 1989) resulted in the neuronal excitation e , which is mostly between zero and one.

The excitation e leads to a neuronal activation u . Neural activation and neuronal excitation are related as formulated by (Zajac, 1989) and as shown in eq. (1).

$$\frac{du(t)}{dt} + \left[\frac{\beta + [1 - \beta]e(t)}{\tau_{act}} \right] \cdot u(t) = \frac{e(t)}{\tau_{act}} \quad (1)$$

$0 < \beta = const. < 1$

The time constant τ_{act} defines the rise time response of the activation. β is a dimensionless parameter that defines the fall time response. τ_{act} (17 ms) and β (0.35) were set, as described in (Grimmelsmann et al., 2023). As a result, two neuronal activations are available, one from the long *biceps* head, one from the short *biceps* head.

2.3 Setup 1: Linear Regression Individually for Each Experiment

For the regression, the neuronal activation of one head of the *biceps* is used as the input. The neuronal activation of the other head of the *biceps* is used as the target. Therefore, there are two possible directions for the regression. From the short head of the *biceps* to the long head of the *biceps* and vice versa.

In the first setup, the regression is done with a linear regression with only the neuronal activation as input. In this setup, the training is done individually for each experiment. This setup should require the least amount of generalisation. For example, the experimental condition *slow, 2kg*, subject id=24 is split into test and training set. The first setup aims to get an impression of the structure and basic dependencies, i.e., how good is the performance of the regression result for the two directions [long to short, short to long] (see fig. 3), by the experiments [[2kg, 4kg], [slow movement, fast movement]] or by the subject numbers [21, ..., 53]. In total, $2 \cdot 2 \cdot 31 = 248$ experiment permutations are possible. However, one experiment failed and is rejected from the used data set.

From the remaining 246 experiment permutations the mean is subtracted and they are scaled to unit variance (standard scaler). After the scaling, the individual experiments are split into 70% training data and 30% test data. The experiments vary in length, but usually last about 30s @ 1.1kHz. The split is based on the sample so the training data contains about 23.000 samples.

In the training process, a linear model is fitted to minimize the residual sum of squares between the targets and the predicted data by the model (Pedregosa et al., 2011). After training, the mean absolute error (MAE) of the test prediction is calculated (in eq. (2)) and presented in section 3.1. The test prediction is the predicted neuronal activation for the test data set.

$$MAE = \frac{\sum_{i=1}^n y_i - x_i}{n} \quad (2)$$

With n is the number of samples, y_i the sample of the predicted value and x_i is the predicted sample.

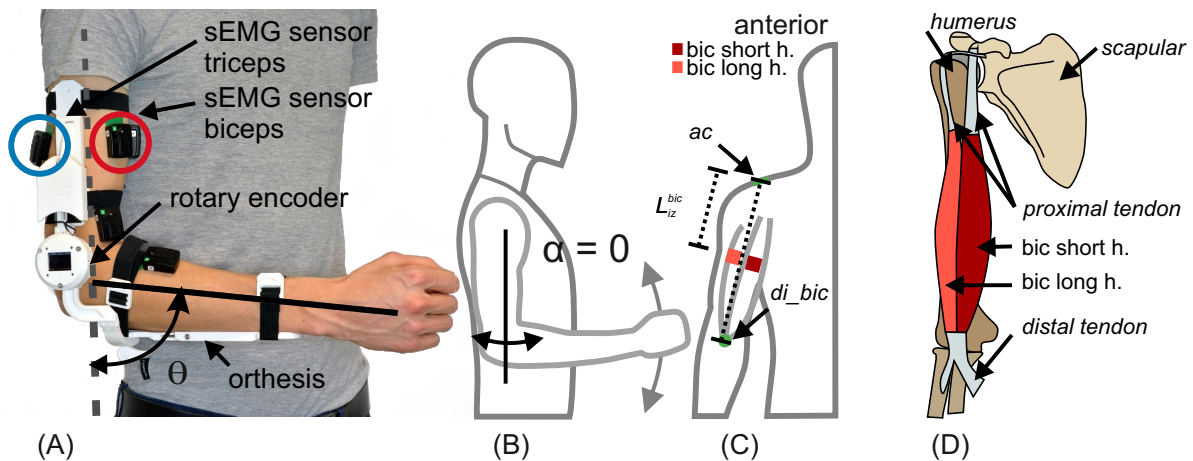


Figure 1: (a) shows the measurement orthosis on the elbow using flexible straps, allowing for adaptation to different subjects. The sEMG sensors were placed on the short and long head of the *biceps* and long and lateral head of the *triceps*, with the wrist rotation in a neutral position. The lower experimental posture is shown in (A) and (B), with the angle of the upper arm (α) being zero (long axis of the upper arm is pointing towards the ground). In (C) the right arm is shown in the coronal plane from an anterior perspective, with the color code of red indicating the *biceps* sensors. The distance from the *acromion* to the innervation zone is also noted. (D) shows a schematic depiction of the long and the short head of the *biceps brachii*. The right shoulder is shown from the anterior perspective. At the top the *scapular* is shown where the two tendons for the individual *biceps* heads are attached. The long head tendon wraps around the *humerus* to add stability to the joint. Whereas the short head is connected to the anterior structure of the *scapular* and links directly down to the muscle belly. At the distal end of the muscle belly, both heads merge into a common tendon. (A), (B), and (C) were adopted and modified from (Grimmelsmann et al., 2023). (D) was modified based on (Schünke et al., 2010).

To be able to evaluate the size of the error, the test prediction is compared to a baseline. To obtain a baseline, the regression output is set to the regression input.

2.4 Setup 2: Leave-One-out, Subject as Variable

In the second setup, the regression is done with (I) a linear regression with only the activation as input, (II) a linear regression with activation, elbow angle, elbow angular velocity, the weight of the dumbbell, and the angle of the upper arm, and (III) a FFN with the rectified linear unit as activation function and the same five inputs as (II). The motivation for these three different configurations was a granular extension of the architecture. The elbow angle is chosen as an input caused by the different utilisation of the muscles over the elbow angle (Chang et al., 1999). One property of the muscle fibre itself is the velocity-dependent force generation. This is why the elbow velocity is taken as an input. The two *biceps* heads attach via their respective tendons to different locations on the shoulder (Schünke et al., 2010). Therefore, the angle of the upper arm has potentially an impact on the activation for the short head of the *biceps*. The long head of the *biceps* needs to stabilise the shoulder more with additional weight

in the hand.

The train/ test split strategy is different from setup 1. Here, the training is performed on all experiments from all subjects excluding all experiments of one subject. This excluded subject is used as the test data set. This training/ test split is done ones for the direction long head to short head and ones for the other direction. As a result, $31 \cdot 2$ training and test sets are created.

The input activation is scaled for each subject with a standard scaler. The elbow angle (θ), the elbow angular velocity (ω), the weight of the dumbbell, and the angle of the upper arm (α) are scaled combined over all subjects again with a standard scaler.

Before training, the activation is filtered with a symmetrical rolling mean. The whole training of setup 2 was optimised using the adam algorithm (Kingma and Ba, 2015) with a learning rate of 0.001 and the MAE as loss function.

2.5 Validation of the Virtual Sensor via a Domain Knowledge Based Model

The model shown in fig. 2 was also used for validation of the virtual sensor but with one input channel (*biceps*) disabled. The remaining *biceps* channel was fed into the model at the point where the neural activation was computed as described in fig. 3(B,C).

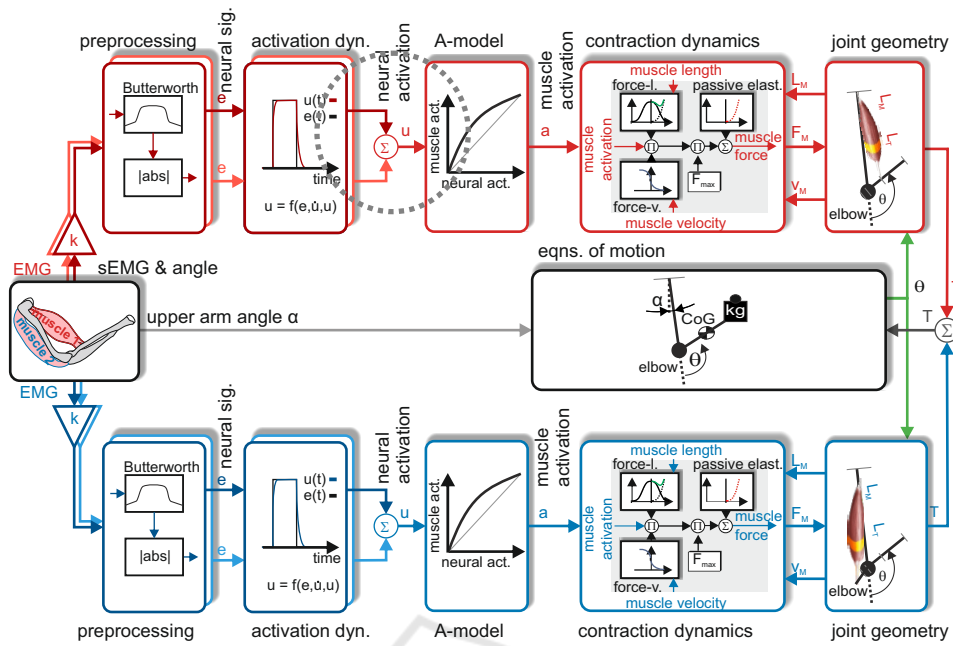


Figure 2: Depiction of the signal flow of the biomechanical model. The biomechanical model which is used to calculate the neuronal activation and to validate the virtual sensor is shown. The signal chart starts on the left with the four sEMG channels. The two *biceps* channels are shown in two shades of red at the top of the arm box. The *triceps* is shown in two shades of blue at the bottom. The sEMG signals are amplified and fed into a preprocessing submodel. The next submodel calculates the neuronal activation for each of the muscle heads. One of these activations is used as an input for the regression. The other activation is used as the target for the regression. In the biomechanical model, the activation is fed into the next submodels until the torque of the *biceps* and the *triceps* sum up to a superimposed torque. This torque is used with dynamics equations to calculate the angle of the elbow. This angle is in the validation step compared to the measured angle. The dotted, grey circle marks the spot where in fig. 3 different structures replace the original structure (Grimmelsmann et al., 2023).

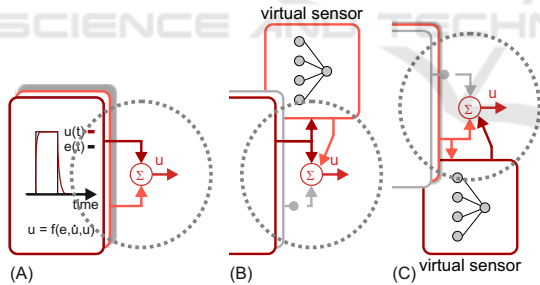


Figure 3: (a) original structure of how neural activation of two heads was added as shown in fig. 2 (cmp. dotted, grey circle). (B) and (C) are the possible replacements for figure (A). (A) uses both neuronal activations from the activation dynamics. (B) shows the structure when using a virtual sensor for the long head of the *biceps*. In (C) the structure is shown for a virtual sensor for the short head of the *biceps*.

This activation was fed into the pre-trained virtual sensor from section 2.4 to get the replacement channel for the disabled one. The performance of the virtual sensor was then measured by comparing the simulated elbow angle θ with the measured elbow angle θ_{meas} . As introduced in (Grimmelsmann et al., 2023), the quality score (QS) was used as a performance indicator. The indicator QS allows

for comparison between different lengths, ranges and shapes of a limb movement. A quality score QS of zero means that no voluntary movement is visible, whereas a QS=1 represents an optimal movement prediction.

Two different configurations can be compared with the baseline. The baseline is the simulation where none of the two *biceps* channels are disabled. Here, all available measured information is used. In the first configuration, the sEMG of the long head was disabled and the activation of this head was provided via the virtual sensor (trained on the direction from short head to long head). In the second configuration, the short head was disabled and the activation was provided via the virtual sensor (trained on the direction long head to the short head).

2.6 sEMG Post Measurement Assessment

The sEMG post measurement assessment was done via the virtual sensor from setup 2 (section 2.4). The goal was to use the general training (on all subject but one) in comparison to the specific test

(only one subject). This is based on the assumption that both biceps heads co-contract as a result of the shared distal tendon. The test prediction from setup 2 was used and plotted to the measured activation. The results are shown in section 3.4 and evaluated manually. This method can be used to provide an idea of the signal quality to an experimenter after or during the sEMG measurement.

3 RESULTS

The result section mirrors the structure of the methods section. First, the results for the regression on individual experiments are shown. After that, the results from the leave-one-out strategy are described. The next part is the validation of the trained sensors by using it in a biomechanical model of the human elbow joint. In the end of the result section the possibility of the sEMG assessment using the introduced method is shown.

3.1 Regression on Individual Experiment Varies Between Subjects

The 246 training MAE and the 246 test MAE of setup 1 show a maximal absolute difference of 0.012. The test errors are sorted in two different ways.

First, they are sorted by the four experiments as shown in fig. 4. The variation between experimental conditions is not significant. Second, the training and test errors are sorted by the subjects. This results in 31 distributions as shown in fig. 5. The individual distributions show greater variations in MAE, in the

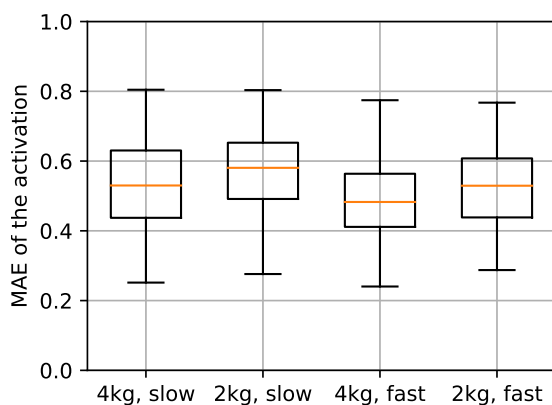


Figure 4: The figure shows the distribution of the MAE over the experiment type in a box and whisker plot. The box marks the interquartile range (IQR), and the whiskers represent data of 1.5· IQR. The MAE for the test set is shown. All four experiments results in similar distributions.

mean as well as also in the range of the distribution. One reason for this is the lower number of data points within each distribution. Compared to the baseline, the performance is only better for some subjects. The subject with the id 28 has a lower MAE compared to the baseline. In contrast to the subject with the id 26 which shows similar MAE values. Some of the subjects (e.g. subject id 26) have significantly lower MAE compared to others. The resulting mean of the MAE for the baseline is equal to mean of the MAE for the virtual sensor (Baseline MAE=0.601, setup 1: virt. short MAE=0.538, virt. long MAE=0.546)

3.2 Small Extension in the Architecture Makes Interpretation Possible

The results for setup 2 are more diverse. The training was performed with all but one subject to obtain a general model, which could then be tested with the left-out subject. The setup contains three different configurations. Configuration (I) is a linear regression with only the activation as input. Configuration (II) is a linear regression with activation, elbow angle, elbow angular velocity, weight of the dumbbell, and the angle of the upper arm. Finally, configuration (III) is a feed-forward net with rectified linear unit as an activation function and the same five inputs as for (II).

The first configuration is a model comparable to the model from setup 1. However, the trained virtual sensor should generalise over more subjects and experiments than in setup 1. The results are shown in fig. 6.

Comparing setup 2 configuration (I) with the baseline shows some performance improvement (baseline MAE=0.601, setup 2 (I): test virt. short MAE=0.476, test virt. long: MAE=0.480, training virt. short: 0.479, training virt. MAE=long: 0.484).

In configuration (II), the input dimension is expanded to five. The additional information leads to larger differences between the two directions for some subjects (e.g. subject ids [32,40]).

The expansion of the input dimension leads to similar MAEs (baseline MAE=0.601, setup 2 (I): test virt. short MAE=0.468, test virt. long: MAE=0.482, training virt. short: 0.465, training virt. MAE=long: 0.481).

The last expansion step in the configuration is to add non-linearity via an activation function (rectified linear unit). The results of this configuration (III) match the trend shown for configurations (I) and (II). The distinction between the two directions is clearer with this extension. The overall training MAE and test MAE are lower than in the previous configurations (baseline MAE=0.601, setup 2 (I) test

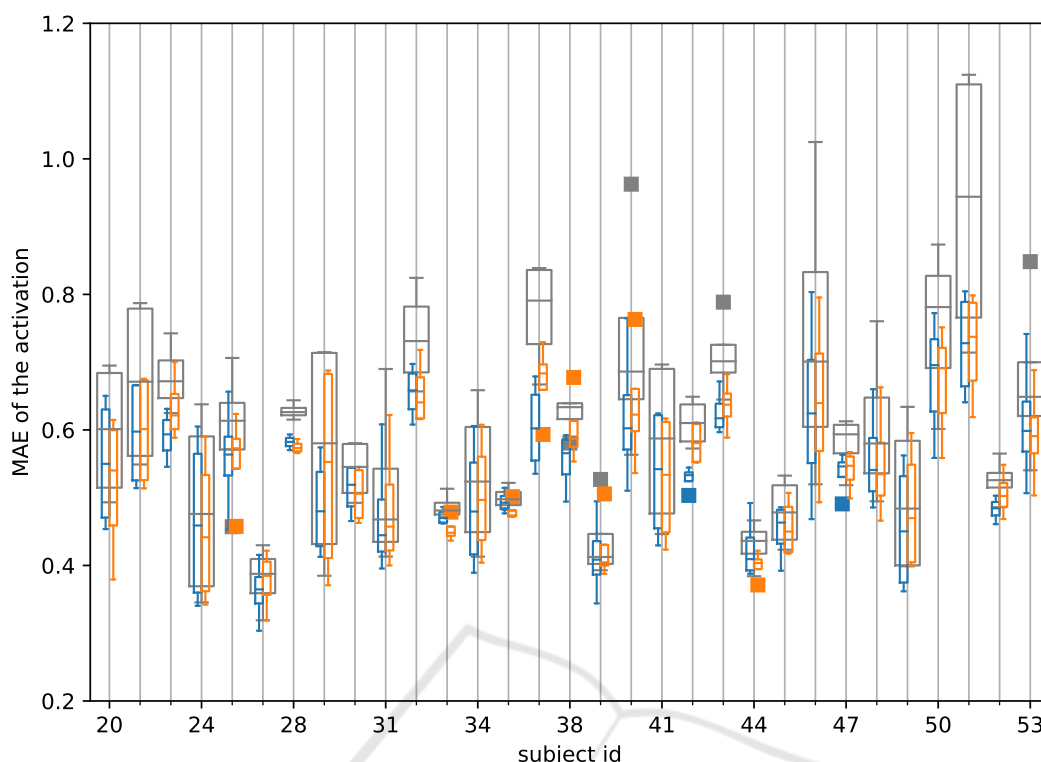


Figure 5: Box and whisker plot of the MAE over the subject id. The general structure is the same as in fig. 4. There are outliers in these distributions marked by boxes. The color represents the direction of the regression. Blue shows the distribution from the virtual sensor for the short head. Orange shows the virtual sensor for the long head. Overall more variation of the median and the IQR is present in this plot. The corresponding data for the training is shown in grey.

virt. short MAE=0.405, test virt. long: MAE=0.367, training virt. short: 0.372, training virt. MAE=long: 0.347).

3.3 The Virtual Sensor Is Viable for Using It in a Biomechanical Model for Movement Prediction

To validate the previously trained virtual sensor, the sensor is used as a replacement input channel in the biomechanical model. For that, the virtual sensor trained with the leave-one-subject-out-strategy and configuration (III) is used. In contrast to the results before, the loss function is replaced by the quality score (QS) between the measured elbow angle and the predicted elbow angle. A higher value means a better result. The data shown in fig. 9 uses the two directions (from long head to short head and vice versa) and the baseline prediction of the biomechanical model. Some variations between these three results are visible for individual subjects. In general, two main trends can be identified. The direction long head to short head tend to increase the prediction performance of the biomechanical model

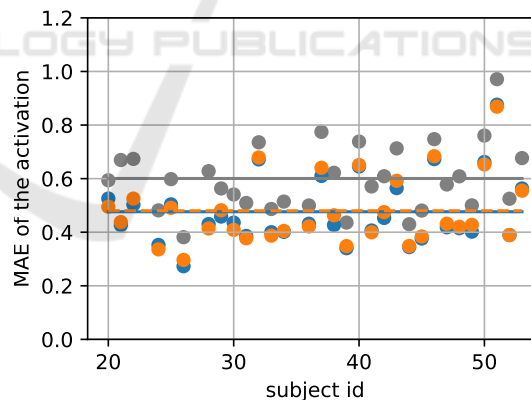


Figure 6: MAE plotted over subject id. The different colors represent the training MAE (grey) and the test MAE for the different directions (from short to long head = orange and vice versa = blue). The lines indicate the mean of the error over all subjects. The subject dependence is similar to the dependence shown in fig. 5. Minor differences between the two directions can be seen for some subjects.

slightly. Using the other direction the biomechanical model shows similar results as with the baseline (both sEMG channels used). The respective values are: baseline: QS=0.324, virt. short: QS=0.346, virt. long: QS=0.324.

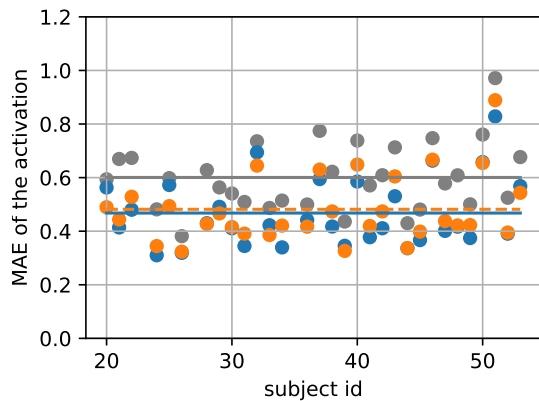


Figure 7: The structure of the figure is the same as fig. 6. The only difference is the underlying data. The overall training MAE and test MAE are similar to configuration (I). The training MAE is slightly lower than the test MAE which indicates a small overfitting.

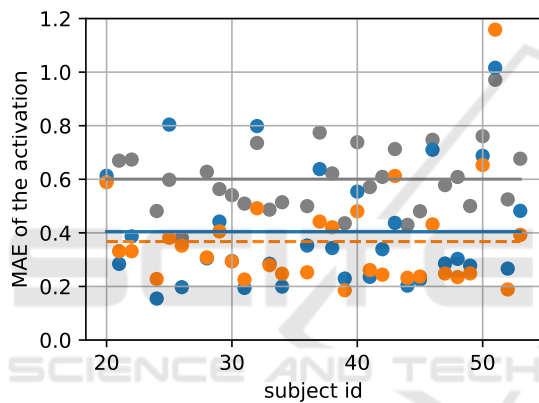


Figure 8: Same structure as figure fig. 6. Configuration (III) is used for the underlying data. This increase in model complexity leads to a better distinction between the directions (from short to long head = orange and vice versa = blue). The training MAE is shown in grey. The lines indicate the mean of the error over all subjects. The loss is generally lower as compared to the other two configurations.

3.4 Virtual Sensor Compared to Measured Signal Can Serve as sEMG Assessment

A deeper analysis of the results from the virtual sensor with configuration (III) allows for an assessment of the sEMG. Therefore, the outputs of the two virtual sensors for the two respective directions were compared. Two exemplary results are chosen from different subjects. Figure 10 shows one of the subjects for which the virtual sensor performed well. The two virtually created activations of this subject are in phase with each other and with the elbow angle.

In contrast to that, the course of the activation

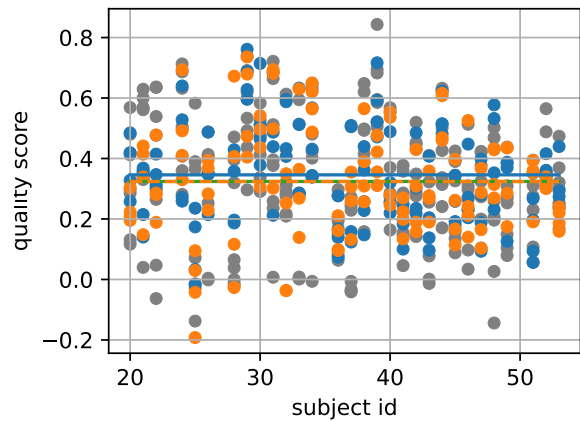


Figure 9: Prediction performance of the biomechanical model utilising: both measured sEMG channel (grey), measured sEMG from the long head plus the virtual sensor for the short head (blue), measured sEMG from the short head plus the virtual sensor for the long head (orange). The subject id is shown vs. the quality score. The mean score is shown as a line over all subject ids.

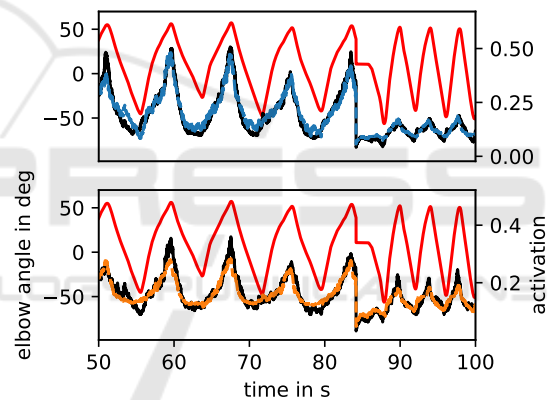


Figure 10: Time series of the two virtual sensors for subject id 24 and the two activations from the measured sEMG. In the upper panel both signals for the short head are shown. The lower panel shows the signals for the long head. The blue line represents the virtual sensor for the virtual long head. In orange the virtual sensor for the short head is shown. As a reference, the angle of the elbow is plotted in red and the activation derived from the measured sEMG plotted in black. The different experiments were concatenated. The discontinuity at time 83s is the change of the experiment.

from the virtual sensor for the two directions can be different for a subject. One of these subjects is shown on fig. 11. Comparing the two virtually created activations for these subjects shows a discrepancy in the phases.

The discrepancy is also present across all experiments. With this plot, the used sEMG can be manually assessed.

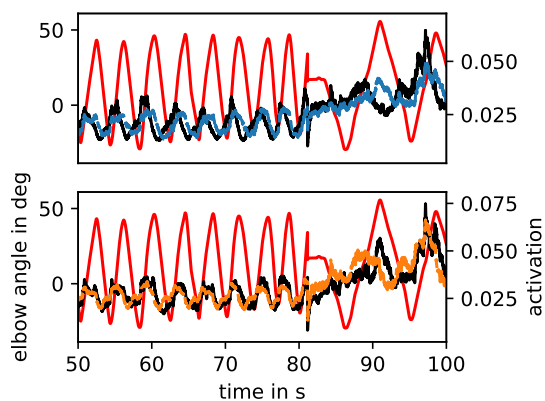


Figure 11: (Cmp. to fig. 10) Time series of the two virtual sensors and the two activation derived from the measured sEMG of subject id 32. The color code is consistent with fig. 10. Here, the experiments changes at time 81s. The activation from the measured short head (black, lower panel) is slightly out of phase. Whereas the activation from the measured long head (black, upper panel) has a higher phase angle. The corresponding virtual sensor shows the same phase. By comparing the measure (black) with the virtual course (blue), the discrepancy is visible.

4 DISCUSSION

In this work, different architectures and training strategies for the regression of two muscle heads are presented. The architecture is expanded from a linear regression with one input to a shallow ffn with five inputs. The presented strategies started with the training based on the individual experiments and ended with the training on all but one subject.

As a result of the regression, virtual sensors are obtained that are suitable as a replacement input to a biomechanical model for limb movement prediction.

The underlying architecture of the virtual sensor contains linear regression and shallow FFN. The results of the linear regression fit the general hypothesis that the two *biceps* heads are usually co-activated in the described experimental paradigm.

Using an architecture with more degrees of freedom, it is possible to differentiate between the two muscle heads. This will be crucial when creating a virtual sensor for a different muscle (like the *brachialis*). Additionally, the virtual sensors generated via leave-one-out learning allow for basic sEMG assessment.

A slight overfitting in the leave-one-out strategy with the configuration (III) is visible. The manual inspection of each test set confirms comparable performance between the training and the test set. One reason for the overfitting could be the relatively high sample frequency of 1.1 kHz.

The results of this study can be used as a simple sEMG assessment tool for data centric AI approaches. The shallow structure of the used FFN allows other researchers to train a similar model for their own data.

Furthermore, the results lay the foundation to push the boundaries of sEMG measurement as a next step. The general problem of measuring deep muscles with sEMG (such as the *brachialis*) may be partially solved by extending the presented method via other architectures beside FFN. In this use case, the virtual sensor will be learned from muscle to muscle to provide a signal of an unknown muscle head for a biomechanical model. A potential time dependency between different muscles activations could require model with a RNN or LSTM architecture.

ACKNOWLEDGEMENTS

This work has been supported by the research training group “Dataninja” (Trustworthy AI for Seamless Problem Solving: Next Generation Intelligence Joins Robust Data Analysis) and by the “TransCareTech” project (Transformation in Care & Technology), both funded by the German federal state of North Rhine-Westfalia.

We would like to thank Philipp Jünemann and Irina Löwen for their valuable contributions during proofreading.

REFERENCES

- Chang, Y.-W., Su, F.-C., Wu, H.-W., and An, K.-N. (1999). Optimum length of muscle contraction. *Clinical Biomechanics*, 14(8):537–542.
- del Toro, S. F., Wei, Y., Olmeda, E., Ren, L., Guowu, W., and Díaz, V. (2019). Validation of a low-cost electromyography (EMG) system via a commercial and accurate EMG device: Pilot study. *Sensors*, 19(23):5214.
- Grimmelsmann, N., Mechtenberg, M., Schenck, W., Meyer, H. G., and Schneider, A. (2023). sEMG-based prediction of human forearm movements utilizing a biomechanical model based on individual anatomical/ physiological measures and a reduced set of optimization parameters. *PLOS ONE*, 18(8):1–28.
- Hill, A. V. (1964). The effect of load on the heat of shortening of muscle. *Proceedings of the Royal Society of London. Series B. Biological Sciences*. Publisher: The Royal Society London.
- Kim, M., Chung, W. K., and Kim, K. (2019). Preliminary Study of Virtual sEMG Signal-Assisted Classification. In *2019 IEEE 16th International Conference on Rehabilitation Robotics (ICORR)*, pages 1133–1138.

- Kingma, D. and Ba, J. (2015). Adam: A method for stochastic optimization. In *International Conference on Learning Representations (ICLR)*, San Diego, CA, USA.
- Koo, T. K. and Mak, A. F. (2005). Feasibility of using emg driven neuromusculoskeletal model for prediction of dynamic movement of the elbow. *Journal of Electromyography and Kinesiology*, 15(1):12–26.
- Leserri, D., Grimmelsmann, N., Mechtenberg, M., Meyer, H. G., and Schneider, A. (2022). Evaluation of semg signal features and segmentation parameters for limb movement prediction using a feedforward neural network. *Mathematics*, 10(6).
- Machado, J. C., Cene, V. H., and Balbinot, A. (2019). Recurrent Neural Network as Estimator for a Virtual sEMG Channel. In *2019 41st Annual International Conference of the IEEE Engineering in Medicine and Biology Society (EMBC)*, pages 3620–3623. IEEE.
- Mechtenberg, M., Grimmelsmann, N., Meyer, H. G., and Schneider, A. (2023). Surface electromyographic recordings of the biceps and triceps brachii for various postures, motion velocities and load conditions. *FH Bielefeld*.
- Merletti, R. and Farina, D. (2008). Analysis of intramuscular electromyogram signals. *Philosophical Transactions of the Royal Society A: Mathematical, Physical and Engineering Sciences*, 367(1887):357–368.
- Merletti, R., Farina, D., and Holobar, A. (2018). *Surface Electromyography (sEMG)*, pages 1–22. John Wiley & Sons, Ltd.
- Pedregosa, F., Varoquaux, G., Gramfort, A., Michel, V., Thirion, B., Grisel, O., Blondel, M., Prettenhofer, P., Weiss, R., Dubourg, V., Vanderplas, J., Passos, A., Cournapeau, D., Brucher, M., Perrot, M., and Duchesnay, E. (2011). Scikit-learn: Machine learning in Python. *Journal of Machine Learning Research*, 12:2825–2830.
- Schünke, M., Schulte, E., Schumacher, U., Voll, M., and Schünke, M. (2010). *Thieme atlas of anatomy: general anatomy and musculoskeletal system; 100 tables*. Thieme, corr. repr., plus version edition.
- Zajac, F. E. (1989). Muscle and tendon: properties, models, scaling, and application to biomechanics and motor control. *Crit Rev Biomed Eng*, 17(4):359–411.